Geometry and energy barrier of martensite in the initial stage martensitic transformation in B19' TiNi shape memory alloy

Teramoto, T.

Nagahira, K.

Tanaka, K.

(Citation)
Acta Materialia,201:94-101

(Issue Date)
2020-12

(Resource Type)
journal article

(Version)
Accepted Manuscript

Geometry and energy barrier of martensite in the initial stage martensitic transformation in B19' TiNi shape memory alloy

T. Teramoto[1], K. Nagahira[1] and K. Tanaka[1]

1. Department of Mechanical Engineering, Kobe University, 1-1 Rokkodai-cho, Nada-ku Kobe, Hyogo 657-8501, Japan

Abstract

This study addresses the selectivity of self-accommodation microstructures in the initial stage of martensitic transformation in B19' TiNi. It is known that specific habit plane variant (HPV) pairs, including $\{11\dot{1}\}_m$type I twin planes that are called initial stage microstructure (ISM) in this study, are preferentially formed in the initial stage of martensitic transformations. To elucidate on the selectivity of the ISM, the energy barrier at the formation of the twin plane, which is the candidate for the starting point of HPV pair formation, and the geometry of the HPV pair are theoretically analyzed in this paper. Using geometrical non-linear theory analysis, the compatible twin plane which has exact twin orientation relationship can be formed in the specific five groups of HPV pair. Using ab-initio simulations and Eshelby theory analysis results, $\{11\dot{1}\}_m$type I twin is determined to have a relatively small energy barrier among the twins in TiNi. Therefore, this paper shows that the HPV pair having a twin plane with a small energy barrier of formation and a structure that can effectively reduce the elastic strain is preferentially formed as the ISM.

1. Introduction

Shape memory alloys, including TiNi alloys, exhibit thermoelastic martensitic transformations that form a characteristic microstructure. It is known that crystallographic features of an individual martensite plate are well described by the phenomenological theory of martensite crystallography (PTMC)[1-6], which is derived by the invariant plane condition at the habit plane between the parent phase and martensite. Four types of equivalent crystallographic correspondence between the parent phase and martensite are derived by PTMC, and each martensite plate is called a habit plane variant (HPV). In the case of TiNi alloy martensites, the lattice invariant deformation required to form the invariant plane is achieved by forming two different lattice correspondence variants (CVs) alternately as an internal twin structure. The aggregates of a HPV forms so as to reduce elastic strain energy caused by an individual variant; this formation is called a self-accommodation microstructure[7].

It is known that martensitic transformation preferentially starts at the grain boundaries of the parent phase. Otherwise, martensites form as a pair of HPVs forming twin boundaries of CVs[8-10]. In the case of TiNi, it has been reported that HPV pairs bounded by $\{11\bar{1}\}_m$type I twins are preferentially formed in the initial stage of martensitic transformation[8] where the subscript "m" indicates that the index is based on the martensite crystal. Indices without the subscript represent the parent crystal throughout this manuscript. The pair of HPVs formed at the initial stage of the martensitic transformation is called the initial stage microstructure (ISM). Figure 1 shows a schematic illustration of the ISM of TiNi. Two HPVs were bounded at the junction plane of the $\{11\bar{1}\}_m$type I twin plane, and each HPV includes a $<011>_m$type II twin in it. Though eight types of possible crystallographic twins exist in the martensite phase of TiNi[11], it is not clear why $\{11\bar{1}\}_m$type I twins are preferentially formed at the formation of ISM.

The geometry and selectivity of the self-accommodation microstructure have been discussed

in several studies. The preferential morphology of the HPVs cluster has been predicted by the arithmetic average of the shape change of HPVs[12-16]. The selectivity of the HPV pair has been predicted by the magnitude of the geometrical misfit at the junction plane between HPVs[17-21]. These past works explain the morphology of the resultant martensite cluster after transformation; however, the kinetics that form the ISM have not yet been clarified. In this study, we investigate the following two factors that control the selectivity of the HPV to form the ISM of the TiNi self-accommodation microstructure.

The first factor is the energy barrier required to form the twin of the martensite phase. When the process forming the second CV with a twin relation at the surface of the first CV is considered, the energy consists of the interfacial energy interface between CV and parent phase, the twin boundary energy, and the elastic energy. Since the ISM has a small volume at the initial stage, it is necessary to discuss the interfacial energy, which is generally considered to have a small effect in the final stage. Since the size of the ISM nuclei is unknown, it is difficult to quantitatively discuss the magnitude of elastic strain energy. However, it is possible to evaluate the relative magnitude of elastic strain energy with different combination of CVs that form twins by calculating the elastic interaction energy with a micromechanics method[22,23].

The second factor is the geometrical aspects of the ISM. The junction plane in the ISM is exactly a $\{11\bar{1}\}_m$type I twin. In general, the interface between two HPVs has “incompatibility” that results from the misorientation due to the exact twin orientation relationship. The incompatibility at the interface is observed in the several self-accommodation microstructures[20,24,25]. The geometrically non-linear theory of martensite crystallography[11,26] (GNLTM) can evaluate the geometry of the incompatibility at the interface. GNLTM analysis has shown that limited HPV pairs can form exact twin orientation relationships. As shown in Figure 1, the junction plane between HPVs is constructed by the local twin planes of CVs. GNLTM analysis of the incompatibility at the local

twin planes in TiNiPd[21] shows that there are two types of interfaces between HPVs: the interface that can form the interface where all local twin planes are compatible, and the interface where incompatibility inevitably exists on the local twin plane. Incompatibility is elastically and plastically relaxed and acts as a source of elastic strain. From the viewpoint of minimizing elastic strain energy, it is assumed that the interface between HPVs without incompatibility is selectively formed as an ISM. For TiNi, the interfaces between HPVs have been crystallographically analyzed and classified in a previous study[19]. However, incompatibility at the local twin planes has not been analyzed, and it has not yet been revealed what HPV pairs can form compatible interfaces.

The aim of this study is to investigate the magnitude relationship of the energy barrier of the twin formation and the incompatibility of the ISM to understand the selectivity of the ISM in TiNi.

2. Analysis procedure

2.1 Twining plane of B19' martensite in TiNi martensitic microstructure

In TiNi, the parent phase has B2 and the martensitic phase has B19'. In the following analysis, the lattice parameters[27] and elastic constants[28,29] in Table 1 were used. Eshelby theory and GNLTM analyses were done in the parent phase lattice coordinate.

There are 12 kinds of CVs. The notation and lattice correspondence of the CVs are summarized in Table 2. All 132 pairs of the CVs are classified into four groups[11]: A, B, C, and D as shown in Figure 2. There are two sets of twins for a given pair of CVs. The notation of the CV pair and the twinning elements are summarized in Table 3. K_1, η_1, K_2 and η_2 are the twinning plane, the twinning direction, the second undistorted conjugate plane and the conjugate twinning direction, respectively.

In TiNi, each HPV contains B-ii as an internal twin and consists of two CVs. In this

study, the CV with a volume fraction that is larger than the other is termed the major CV, and the other is termed the minor CV. HPV is characterized by contained CVs and the habit plane orientation. In this study, HPV constructed by major CV*i* and minor CV*j* is termed (*i-j*). In TiNi, there are 24 kinds of HPVs.

2.2 Elastic interaction energy between CVs

The elastic interaction energy between CVs is evaluated on the basis of Eshelby theory[22,23] for anisotropic inclusion. Because the volume of a CV is extremely small in the initial stage of the martensitic transformation, the shape of a CV was approximated by a unit ball in this study. The center of a CV*i* is placed at the origin. To investigate the orientation dependence of the elastic interaction energy at the surface of CV*i*, the center of CV*j* is placed at a 1.01 distance at all points from the origin. The elastic interaction energy between CV*i* and CV*j* per unit volume is expressed as;

$$E_{i\text{-}j} = -\sigma^{i}_{pq}(\boldsymbol{x})\varepsilon^{j}_{pq} \qquad \text{Eq. 1}$$

where $\sigma^{i}_{pq}(\boldsymbol{x})$ is the internal stress due to the CV*i*, ε^{j}_{pq} is the eigenstrain that corresponds to the transformation strain of CV*j*, $\boldsymbol{x}$ is the center position of CV*j*, and the origin of the $\boldsymbol{x}$ is at center of CV*i*. $\sigma^{i}_{pq}(\boldsymbol{x})$ outside of CV*i* has been given by Mura and Cheng[30].

2.3 Interfacial energy

The interfacial energy of the twin plane was evaluated by ab-initio simulations. Density functional theory simulations were performed with the Vienna Ab-initio Simulation Package (VASP)[31-34] using the projector augmented wave method (PAW)[35,36] and the generalized gradient approximation proposed by Perdew, Burke, and Ernzerhof (GGA-PBE)[37].

The interfacial energy is defined as the change in the total energy upon the addition of

twinning plane. The interfacial energy is expressed by the following equation[38];

$$\gamma = (F_{\text{twin}} - F_{\text{B19'}})/2A \qquad \text{Eq. 2}$$

F_{twin} and $F_{\text{B19'}}$ are the total energy of the cell, including the twin plane and bulk cell of the martensitic phase. A is the area of the twin plane. The principal axes, size of the cell, k-mesh, total number of atoms are summarized in Table 4. The cells were created in the coordinate system of ($\boldsymbol{v}_1$, $\boldsymbol{v}_2$, $\boldsymbol{v}_3 = \boldsymbol{v}_1 \times \boldsymbol{v}_2$). D is the distance between twin planes along the plane normal of the twin plane $\boldsymbol{v}_3$. The Monkhorst–Pack mesh of k points were used to integrate the Brillouin zone. The plane-wave cutoff energy and the energy convergence criterion (ECC) during the electronic self-consistency loop were set to 400 eV and 10^{-6}eV, respectively. The condition of ECC=10^{-7}eV has been used in the previous studies[39,40] on ab initio simulations of TiNi. The number of atoms in the cells including twin plane are large, and a long computation time is required for analysis. We do not focus on the accuracy of the interfacial energy, but rather on elucidating the relationship between the size of the interfacial energy. Therefore, the calculations were performed under the relatively weak energy convergence criterion. The influence of the free energy convergence criterion on the total energy of the TiNi single phase is shown in Table 5. These calculations were performed with the k-points grid (11×11×11) and the cutoff energy of 500eV. The calculation with ECC=10^{-6}eV, which is used to calculate the cell including twin plane, results in an error of about 10^{-4}eV in the total energy compared to the calculation with ECC=10^{-8}eV. This error is considered to generate an error of about 2 mJ/m^2 in the interfacial energy. The difference of the interfacial energy between the twin plane is tens of mJ/m^2, which is sufficiently accurate to discuss the magnitude relationship of the interfacial energy. The atomic positions and the shape of cell including twin plane were optimized using the internal VASP procedure. The $(11\bar{1})_{\text{m}}$type I twin cell after the relaxation and the Ti atom displacement from B19' bulk crystal in each layer are shown in Figure 3 as an example. Due to the relaxation of the twin plane structure, the cell,

including the twin, has a relaxed area near the twin plane. To suppress the interaction of the twin planes, the cells with sufficient twin plane spacing were used for calculation.

Although the B19' structure has been observed experimentally in TiNi, the orthorhombic B33 structure is reported to be the lowest energy structure in the ground state in the previous studies[39,40,41]. It is assumed that the adoption of the B19' structure generates stresses in the cell and affects the interfacial energy at the twin interface. However, we adopt the B19' structure to analyze the interfacial energy of the experimentally observed twin plane in order to elucidate the selectivity of the experimentally observed ISM. Therefore, it should be noted that the interfacial energy analyzed in this study is different from the interfacial energy of the lowest energy structure in the ground state. Visualization of the cells was performed with visualization for electronic and structural analysis (VESTA)[42].

2.4 Incompatibility at the twin planes

Incompatibility at the twin plane between CVs and the interface between HPVs was evaluated by the kinematic compatibility (KC) condition[26]. The KC condition at the interface between two homogeneously deformed domains (Ω_i and Ω_j) is expressed as the following equation:

$$\mathbf{R}\mathbf{D}_j - \mathbf{D}_i = \mathbf{d}\otimes\mathbf{v} \qquad \text{Eq. 3}$$

$\mathbf{D}_i$ and $\mathbf{D}_j$ are the deformation gradients of Ω_i and Ω_j, respectively. **R** is incompatibility, which is the rigid rotation of $\mathbf{D}_j$ required for the KC condition with $\mathbf{D}_i$ at the interface.

The deformation gradient of (*i-j*) is expressed as following equations:

$$\mathbf{Q}\mathbf{B}_j - \mathbf{B}_i = \mathbf{a}\otimes\mathbf{n} \qquad \text{Eq. 4}$$

$$\mathbf{U}_{(i\text{-}j)} = \mathbf{Q}'\left(\lambda\mathbf{Q}\mathbf{B}_j + (1-\lambda)\mathbf{B}_i\right) = \mathbf{I} + \mathbf{b}\otimes\mathbf{m} \qquad \text{Eq. 5}$$

$\mathbf{B}_i$ is a deformation gradient of CV*i*, which is calculated by the lattice parameters. **a** and **n** are the

vectors that describe the shear direction and twin interface normal of the internal twin. **Q** and **Q**' are additional rotations for the KC conditions. λ is the volume fraction of the minor CV*j*. $\mathbf{U}_{(i,j)}$ and **I** is the deformation gradient of (*i-j*) and identity matrix. **b** and **m** are the vectors that describe the shape change direction and habit plane normal. Since CV*i* and CV*j* in the (*i-j*) are rotated by the additional rotation, the deformation gradients of CV*i* and CV*j* are expressed by the following equations:

$$\mathbf{V}_i = \mathbf{Q'B}_i \qquad \text{Eq. 6}$$

$$\mathbf{V}_j = \mathbf{Q'QB}_j \qquad \text{Eq. 7}$$

$\mathbf{V}_i$ and $\mathbf{V}_j$ are the deformation gradients of major CV*i* and minor CV*j*. Incompatibility in the junction plane between HPVs and the twin plane between CVs were calculated using Eq. 3 with the deformation gradients of HPV and CV.

3. Results

3.1 Elastic interaction energy of the twins between CVs

Elastic interaction energies were analyzed for all CV pairs in Table 3. Figure 4 shows the orientation dependence of E_{i-j} for each CV pair. The solid line indicates the line of $E_{i-j} = 0$, and the index of the twin plane is indicated by a white point. The area where E_{i-j} is negative indicates that the formation of CV*j* was elastically favored in this area. All twin planes were located in a region where E_{i-j} was negative. The E_{i-j} at the twin plane normal for each CV pair is summarized in Table 6. All twin planes between CVs have a negative value of E_{i-j} which means they are elastically stable. Except for D-ii, the E_{i-j} of each twin has the same order in the magnitude. The twin planes with especially small E_{i-j} are A-c1, B-i, and C-i. All twin planes between CVs were elastically stable, and it is assumed that the ISMs including A-c1, B-i, and C-i had the minimum

elastic strain energy barrier.

3.2 Interfacial energy of the twin planes

In this study, the interfacial energies of type I twins (B-i, C-i and D-i) and compound twins (A-c1 and A-c2) were analyzed. The twin plane of type II twin is an irrational plane. The structure of the type II twin plane has been reported as a ledged-terraced structure[40][41] or randomly curved structure[42,43]. In conclusion, the structure of the twin plane is not clear. Therefore, it is difficult to apply the first-principle calculations for the analysis of the type II twin. Interfacial energy analysis of type II twins was not performed in this study. The treatment of the type II twins is described in the discussion. Calculated interfacial energies are summarized in Table 7.

3.3 Geometry of a twin

There are 552 pairs of twins between HPVs. Of all pairs, 216 can form twin planes between HPVs that are classified into nine groups as summarized in Figure 5. In Figure 5, I–XI indicate group numbers, and blanks indicate that the pair cannot form a twin plane. The geometry of incompatibility between HPVs, major-CVs, and minor-CVs of group I–IX are summarized in Table 8. In Table 8, $\mathbf{n}_{ij}$ is a vector that describes twin plane normal. θ and $\mathbf{\Gamma}$ are the rotation angle and the rotation axis of the incompatibility. Twin type indicates the twin type of the local twin plane. There are two sets of solutions for a given pair of HPVs. The notation of each solution is expressed as No. in Table 8.

The interface between HPVs is constructed by the local twin planes between CVs. There are three types of local twin planes: twin planes between major CVs (major twin), twin planes between minor CVs (minor twin), and twin planes between major CV and minor CV (major-

minor twin). Since the CVs in HPV are not able to rotate individually, the geometry of incompatibility at all local twin planes must be the same to eliminate incompatibility at all local twin planes. II-2 corresponds to this type. The elimination of the major-minor twin is accomplished by the one-to-one connection between major CVs and the one-to-one connection between minor CVs. In this situation, the geometry of incompatibility at the major twin and the minor twin must be the same to form the compatible twin plane. I-1, III-1, VI-1, and VII-1 correspond to this type.

4. Discussion

As shown in Table 6 B-i, A-c1 and C-i have the minimum elastic interaction energy. Therefore, the elastic strain energy term of the energy barrier of the twin plane formation is the minimum in B-i, A-c1 and C-i. As shown in Table 7, B-i and C-i have the minimum interfacial energy among the type I and compound twins. In this study, the interfacial energies of type II twins are not analyzed, and the magnitude relation of the interfacial energies with other kind of twins is not clear. However, since type II twin planes have a complex structure, the area of twin plane per unit volume is larger than that of the type I or the compound twin plane. It is assumed that the complex structure interface has a relatively high interfacial energy per unit area. Therefore, the interfacial energy term of the energy barrier of the twin plane formation is the minimum in B-i and C-i. In summary, B-i and C-i are considered to be twin planes where both the elastic strain energy term and the interfacial energy term of the energy barrier are small and have a relatively small energy barrier compared to the other twins.

In the compatible HPV pairs (I-1, II-2, III-1, VI-1, and VII-1), incompatibility is the rigid rotation of $HPV_{(k\text{-}l)}$ to form the exact twin plane. The rotation of the HPV breaks the invariant

plane condition at the habit plane and generates the misfit at the habit plane. Since the misfit is elastically and plastically relaxed, it is assumed that the rotation angle of the incompatibility is an index of the magnitude of the elastic strain when the ISM grows. The rotation angle of II-2, III-1, and VII-1 are an order smaller than that of I-1 and VI-1. Therefore, II-2, III-1, and VII-1 can form exact twin planes and have small elastic strain energy during growth. II-2, III-1, and VII-1include B-ii, A-c1, and C-i. Among these twin planes, C-i is considered to be the twin plane with the smallest energy barrier. VII-1, including C-i, is the ISM that is observed in in-situ observations[8]. One-to-one connections of major CVs and minor CVs are necessary to form the compatible junction plane of VII-1. The observed structure[18] of ISM has the one-to-one connection structure that is predicted by GNLTM analysis in this study. Therefore, it has been shown that the HPV pair having the twin plane with a small elastic energy barrier and a structure that can effectively reduce the incompatibility is preferentially formed as the ISM.

5. Conclusions

To understand the selectivity of the IMS, the magnitude relationship between the energy barrier of the twin formation and the incompatibility of the ISM have been investigated for TiNi B19’ martensite. There are nine distinct types of HPV pairs and three types of HPV paris (II-2, III-1, and VII-1) that can eliminate the incompatibility at the junction plane by a relatively small rigid rotation. II-2, III-1, and VII-1 include B-ii, A-c1, and C-i type twin planes between CVs,. B-i and C-i are considered to be twin planes where both the elastic strain energy term and the interfacial energy term of the energy barrier are small and have a relatively small energy barrier compared to the other twins. VII-1, including C-i, is suitable for the type of ISM that is observed in the actual microstructure. Therefore, the HPV pair having a twin plane that has a small energy barrier of formation and the structure that can effectively reduce incompatibility is

preferentially formed as the ISM.

Acknowledgements

This work was supported by the Grants-in-Aid for Scientific Research (Grant Number 17K14843) from the Japan Society for the Promotion of Science.

References

[1] J.S. Bowles, J.K. Mackenzie, The crystallography of martensite transformations I, Acta Metall. 2 (1954) 129–137.

[2] J.. Mackenzie, J.. Bowles, The crystallography of martensite transformations II, Acta Metall. 2 (1954) 138–147.

[3] J.S. Bowles, J.K. Mackenzie, The crystallography of martensite transformations III. Face-centred cubic to body-centred tetragonal transformations, Acta Metall. 2 (1954) 224–234.

[4] J.K. Mackenzie, J.S. Bowles, The crystallography of martensite transformations-IV body-centred cubic to orthorhombic transformations, Acta Metall. 5 (1957) 137-149.

[5] M.S. Wechsler, D.S. Lieberman, T.A. Read, On the theory of the formation of martensite, Trans. AIME. 197 (1953) 1503–1515.

[6] D.S. Lieberman, M.S. Wechsler, T.A. Read, Cubic to orthorhombic diffusionless phase change - Experimental and theoretical studies of AuCd, J. Appl. Phys. 26 (1955) 473–484.

[7] K. Otuska and C. M. Wayman, Shape Memory Materials, Cambridge University Press, Cambridge, 1998.

[8] Y. Soejima, S. Motomura, M. Mitsuhara, T. Inamura, M. Nishida, In situ scanning electron microscopy study of the thermoelastic martensitic transformation in Ti-Ni shape

memory alloy, Acta Mater. 103 (2016) 352-360.

[9] M. Ueda, H.Y. Yasuda, Y. Umakoshi, Controlling factor for nucleation of martensite at grain boundary in Fe-Ni bicrystals, Acta Mater. 51 (2003) 1007-1017.

[10] T. Inamura, M. Ii, M. Tahara, H. Hosoda, Formation process of the incompatible martensite microstructure in a beta-titanium shape memory alloy, Acta Mater. 124 (2017) 351-359.

[11] K. Bhattacharya, Microstructure of Martensite, Oxford University Press, New York, 2003.

[12] T. Saburi, C.M. Wayman, Crystallographic similarities in shape memory martensites, Acta Metall. 27 (1979) 979-995.

[13] K. Otsuka, K. Shimizu, MORPHOLOGY AND CRYSTALLOGRAPHY OF THERMOELASTIC Cu-Al-Ni MARTENSITE ANALYZED BY THE PHENOMENOLOGICAL THEORY., Trans Jap Inst Met. 15 (1974) 103–108.

[14] S. Miyazaki, K. Otsuka, C.M. Wayman, The shape memory mechanism associated with the martensitic transformation in Ti-Ni alloys—II. Variant coalescence and shape recovery, Acta Metall. 37 (1989) 1885–1890.

[15] S. Miyazaki, K. Otsuka, C.M. Wayman, The shape memory mechanism associated with the martensitic transformation in TiNi alloys-I. Self-accommodation, Acta Metall. 37 (1989) 1873–1884.

[16] K. Madangopal, The self accommodating martensitic microstructure of Ni-Ti shape memory alloys, Acta Mater. 45 (1997) 5347–5365.

[17] M. Nishida, T. Nishiura, H. Kawano, T. Inamura, Self-accommodation of B19′ martensite in Ti-Ni shape memory alloys-Part I. Morphological and crystallographic studies of the variant selection rule, Philos. Mag. 92 (2012) 2215–2233.

[18] M. Nishida, E. Okunishi, T. Nishiura, H. Kawano, T. Inamura, S. Ii, T. Hara, Self-accommodation of B19 martensite in Ti-Ni shape memory alloys-Part II. Characteristic interface structures between habit plane variants, Philos. Mag. 92 (2012) 2234–2246.

[19] T. Inamura, T. Nishiura, H. Kawano, H. Hosoda, M. Nishida, Self-accommodation of B19′ martensite in Ti-Ni shape memory alloys. Part III. Analysis of habit plane variant clusters by the geometrically nonlinear theory, Philos. Mag. 92 (2012) 2247–2263.

[20] T. Inamura, H. Hosoda, S. Miyazaki, Incompatibility and preferred morphology in the self-accommodation microstructure of β-titanium shape memory alloy, Philos. Mag. 93 (2013) 618–634.

[21] T. Teramoto, M. Tahara, H. Hosoda, T. Inamura, Compatibility at junction planes between habit plane variants with internal twin in Ti-Ni-Pd shape memory alloy, Mater. Trans. 57 (2016) 233–240.

[22] J.D. Eshelby, The determination of the elastic field of an ellipsoidal inclusion, and related problems, Proc. R. Soc. London. Ser. A. Math. Phys. Sci. 241 (1957) 376–396.

[23] T. Mura, Micromechanics of defects in solids, Springer Netherlands, Dordrecht, 1987.

[24] K. Adachl, J. Perkins, C.M. Wayman, The crystallography and boundary structure of interplate-group combinations of 18R martensite variants in Cu-Zn-Al shape memory alloys, Acta Metall. 36 (1988) 1343-1364.

[25] K. Adachi, J. Perkins, C.M. Wayman, Type II twins in self-accommodating martensite plate variants in a CuZnAl shape memory alloy, Acta Metall. 34 (1986) 2471-2485.

[26] J.M. Ball, R.D. James, Fine phase mixtures as minimizers of energy, Arch. Ration. Mech. Anal. 100 (1987) 13–52.

[27] Y. Kudoh, M. Tokonami, S. Miyazaki, K. Otsuka, Crystal structure of the martensite in Ti-49.2 at.%Ni alloy analyzed by the single crystal X-ray diffraction method, Acta

Metall. 33 (1985) 2049-2056.

[28] N. Hatcher, O.Y. Kontsevoi, A.J. Freeman, Role of elastic and shear stabilities in the martensitic transformation path of NiTi, Phys. Rev. B. 80 (2009) 144203.

[29] O. Mercier, K.N. Melton, G. Gremaud, J. Hägi, Single□crystal elastic constants of the equiatomic NiTi alloy near the martensitic transformation, J. Appl. Phys. 51 (1980) 1833–1834.

[30] T. Mura, P.C. Cheng, The Elastic Field Outside an Ellipsoidal Inclusion, J. Appl. Mech. 44 (1977) 591–594.

[31] G. Kresse, J. Hafner, Ab initio molecular dynamics for liquid metals, Phys. Rev. B. 47 (1993) 558–561.

[32] G. Kresse, J. Hafner, Ab initio molecular-dynamics simulation of the liquid-metal–amorphous-semiconductor transition in germanium, Phys. Rev. B. 49 (1994) 14251–14269.

[33] G. Kresse, J. Furthmüller, Efficient iterative schemes for ab initio total-energy calculations using a plane-wave basis set, Phys. Rev. B. 54 (1996) 11169–11186.

[34] G. Kresse, J. Furthmüller, Efficiency of ab-initio total energy calculations for metals and semiconductors using a plane-wave basis set, Comput. Mater. Sci. 6 (1996) 15–50.

[35] P.E. Blöchl, Projector augmented-wave method, Phys. Rev. B. 50 (1994) 17953–17979.

[36] G. Kresse, D. Joubert, From ultrasoft pseudopotentials to the projector augmented-wave method, Phys. Rev. B. 59 (1999) 1758–1775.

[37] J.P. Perdew, K. Burke, M. Ernzerhof, Generalized Gradient Approximation Made Simple, Phys. Rev. Lett. 77 (1996) 3865–3868.

[38] L. Sandoval, J.B. Haskins, J.W. Lawson, Stability, structure, and suppression of the martensitic transition temperature by B19′ compound twins in NiTi: ab initio and

classical simulations, Acta Mater. 154 (2018) 182-189.

[39] M. F. X. Wagner, W. Windl, Acta Mater. 56 (2008) 6232-6245.

[40] P. Sestak, M. Cerny, J. He, Z. Zhang, J. Pokluda, Acta Mater. 109 (2016) 223-229.

[41] X. I. Huang, G. J. Ackland, K. M. Rabe, Nat. Mater. 2 (2003) 307-311.

[42] K. Momma, F. Izumi, VESTA 3 for three-dimensional visualization of crystal, volumetric and morphology data, J. Appl. Crystallogr. 44 (2011) 1272–1276.

[43] Z.L. Xie, Y. Liu, HRTEM study of □011□ type II twin in NiTi shape memory alloy, Philos. Mag. 84 (2004) 3497–3507.

[44] K.M. Knowles, A high-resolution electron microscope study of nickel-titanium martensite, Philos. Mag. A. 45 (1982) 357–370.

[45] M. Nishida, H. Ohgi, I. Itai, A. Chiba, K. Yamauchi, Electron microscopy studies of twin morphologies in B19′ martensite in the Ti-Ni shape memory alloy, Acta Metall. Mater. 43 (1995) 1219–1227.

[46] T. Onda, Y. Bando, T. Ohba, K. Otsuka, Electron Microscopy Study of Twins in Martensite in a Ti-50.0 at%Ni Alloy, Mater. Trans. JIM. 33 (1992) 354–359.

Figures and Tables

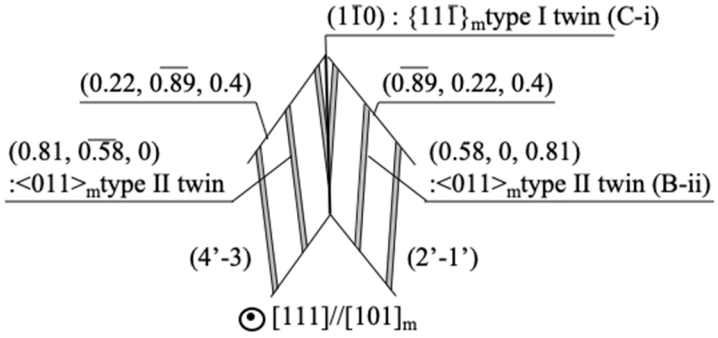

Figure 1 Schematic image of ISM in TiNi.

{11$\bar{1}$}$_m$type I twin and <011>$_m$type II twin correspond to C-i and B-ii in Table3

CV*i*

CV*j*	1	1'	2	2'	3	3'	4	4'	5	5'	6	6'
1		A	B	B		D	C			C		D
1'	A		B	B	C			D	D		C	
2	B	B		A		C	D		C		D	
2'	B	B	A		D			C		D		C
3		C		D		A	B	B		D	C	
3'	D		C		A		B	B	C			D
4	C		D		B	B		A		C	D	
4'		D		C	B	B	A		D			C
5		D	C			C		D		A	B	B
5'	C			D	D		C		A		B	B
6		C	D		C		D		B	B		A
6'	D			C		D		C	B	B	A	

Figure 2 Classification of twin between CVs

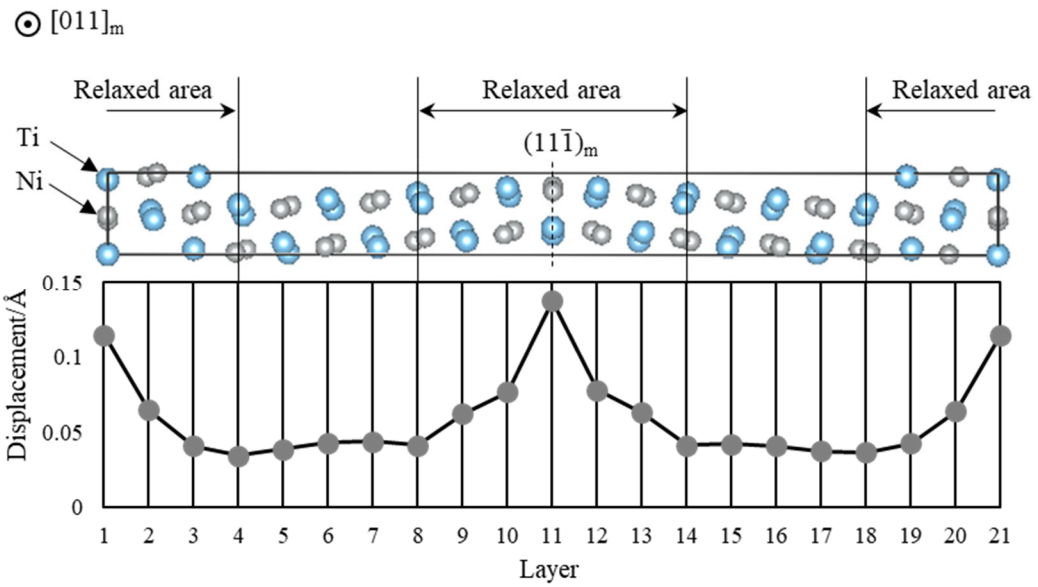

Figure 3 Relaxation of the cell including $(11\dot{1})_m$type I twin plane in ab-initio simulation

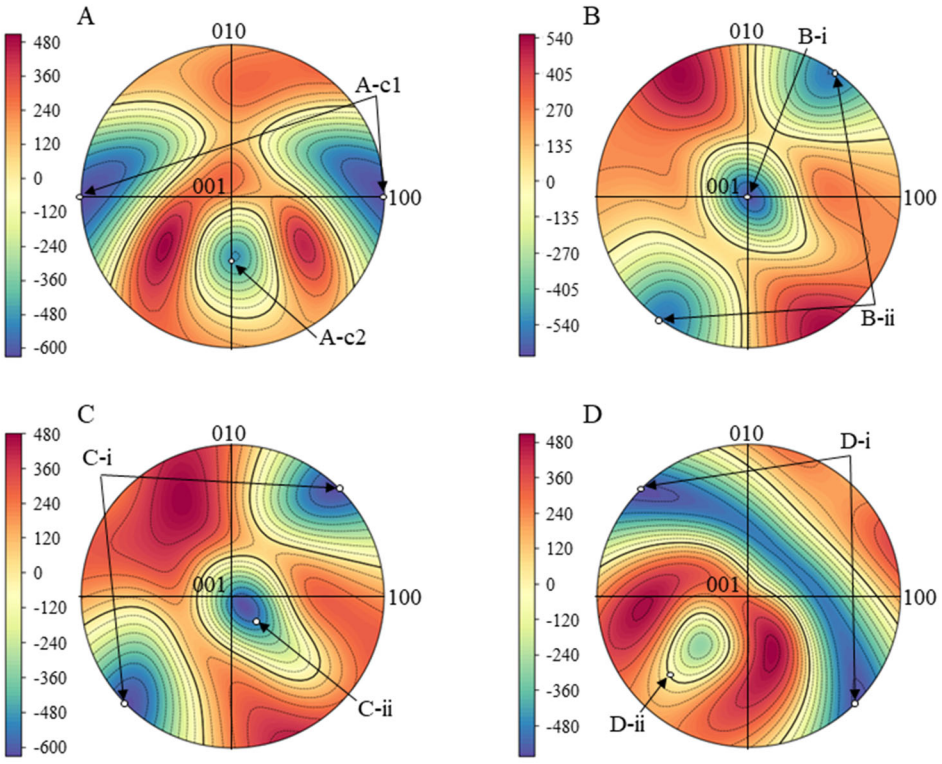

Figure 4 Orientation dependence of the elastic interaction energy $E_{i\text{-}j}$

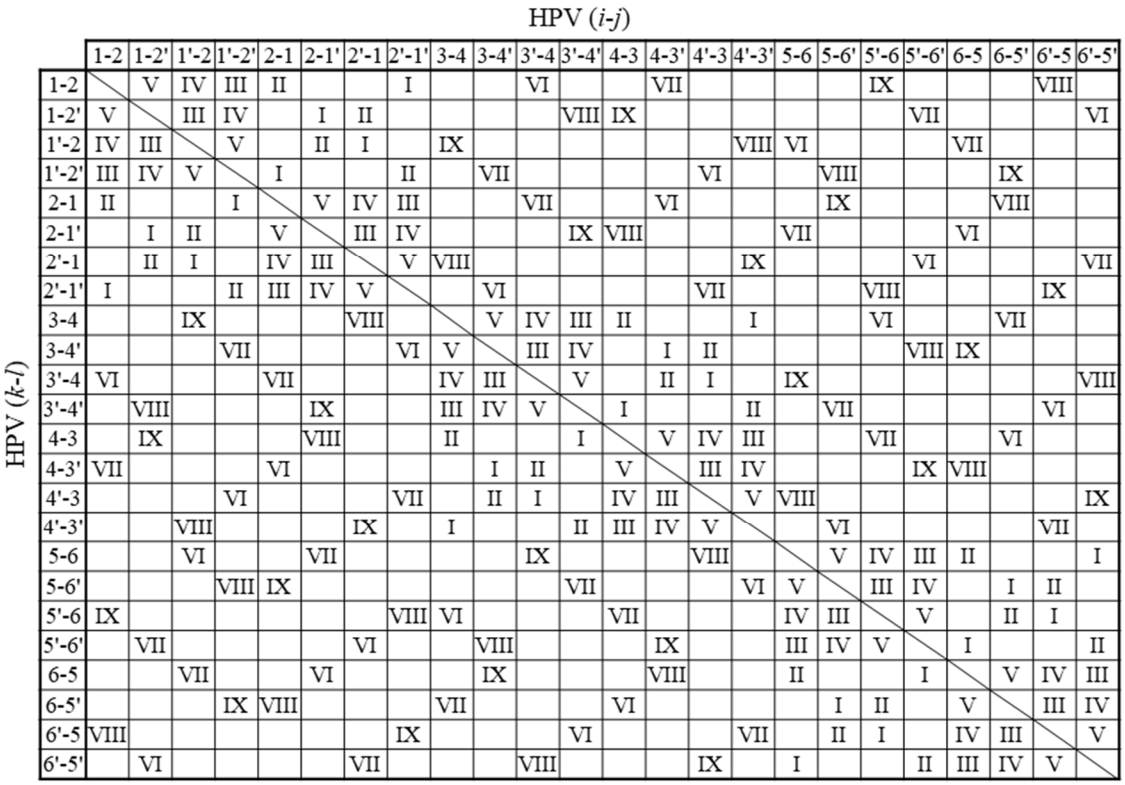

Figure 5 Classification of HPV pair

Table 1 Lattice parameters and elastic constants of TiNi

	B2 (Parent phase)	B19' (Martensitic phase)
Lattice parameter (nm)	$p = 0.3015$	$a = 0.2889, b = 0,4120, c = 0.4622$ $\beta = 96.8^{o}$
Elastic constants (GPa)	$c_{11} = c_{22} = c_{33} = 162.0$ $c_{12} = c_{13} = c_{23} = 129.0$ $c_{44} = c_{55} = c_{66} = 34.0$	$c_{11} = 249, c_{22} = 245, c_{33} = 212$ $c_{12} = 129, c_{13} = 107, c_{15} = 15$ $c_{23} = 125, c_{25} = -3, c_{35} = -1$ $c_{44} = 87, c_{46} = -4, c_{55} = 66, c_{66} = 86$

Table 2 Lattice correspondence of CV

CV	$[100]_m$	$[010]_m$	$[001]_m$
1	[100]	[011]	$[0\bar{1}1]$
1'	$[\bar{1}00]$	$[0\bar{1}\bar{1}]$	$[0\bar{1}1]$
2	[100]	$[0\bar{1}1]$	$[0\bar{1}\bar{1}]$
2'	$[\bar{1}00]$	$[01\bar{1}]$	$[0\bar{1}\bar{1}]$
3	[010]	[101]	$[10\bar{1}]$
3'	$[0\bar{1}0]$	$[\bar{1}0\bar{1}]$	$[10\bar{1}]$
4	[010]	$[10\bar{1}]$	$[\bar{1}0\bar{1}]$
4'	$[0\bar{1}0]$	$[\bar{1}01]$	$[\bar{1}0\bar{1}]$
5	[001]	[110]	$[\bar{1}10]$
5'	$[00\bar{1}]$	$[\bar{1}\bar{1}0]$	$[\bar{1}10]$
6	[001]	$[\bar{1}10]$	$[\bar{1}\bar{1}0]$
6'	$[00\bar{1}]$	$[1\bar{1}0]$	$[\bar{1}\bar{1}0]$

Table 3 Notation and twinning elements of twins between CVs

CV*i* - CV*j*	Group	No.	K_1	η_1	K_2	η_2	s
1 - 1'	A	A-c1 A-c2	$(1,0,0)_m$ $(0,0,1)_m$	$[0,0,1]_m$ $[1,0,0]_m$	$(0,0,1)_m$ $(1,0,0)_m$	$[1,0,0]_m$ $[0,0,1]_m$	0.24
1 - 2	B	B-i B-ii	$(0,1,1)_m$ $(0.72,1,\bar{1})_m$	$[1.57,1,\bar{1}]_m$ $[0,1,1]_m$	$(0.72,1,\bar{1})_m$ $(0,1,1)_m$	$[0,1,1]_m$ $[1.57,1,\bar{1}]_m$	0.28
1 - 4	C	C-i C-ii	$(1,1,\bar{1})_m$ $(0.25,0.51,1)_m$	$[1.18,1,2.18]_m$ $[2,1,\bar{1}]_m$	$(0.25,0.51,1)_m$ $(1,1,\bar{1})_m$	$[2,1,\bar{1}]_m$ $[1.18,1,2.18]_m$	0.31
1 - 3'	D	D-i D-ii	$(1,\bar{1},1)_m$ $(0.67,0.34,\bar{1})_m$	$[2.95,1,\overline{1.95}]_m$ $[2,\bar{1},1]_m$	$(0.67,0.34,\bar{1})_m$ $(1,\bar{1},1)_m$	$[2,\bar{1},1]_m$ $[2.95,1,\overline{1.95}]_m$	0.14

Table 4 Calculation condition and cells of the interfacial energy analysis

	Principal axes in twin plane	D (nm)	k-mesh	Number of atoms
A-c1	$\boldsymbol{v}_1 = [010]_m$, $\boldsymbol{v}_2 = [001]_m$	2.87	6×6×1	80
A-c2	$\boldsymbol{v}_1 = [100]_m$, $\boldsymbol{v}_2 = [010]_m$	2.76	9×6×1	48
B-i	$\boldsymbol{v}_1 = [100]_m$, $\boldsymbol{v}_2 = [01\bar{1}]_m$	2.45	8×4×1	64
B-ii	N/A			
C-i	$\boldsymbol{v}_1 = [011]_m$, $\boldsymbol{v}_2 = [\bar{1}10]_m$	2.20	4×5×1	80
C-ii	N/A			
D-i	$\boldsymbol{v}_1 = [110]_m$, $\boldsymbol{v}_2 = [\bar{1}01]_m$	2.21	5×4×1	88
D-ii	N/A			

Table 5 Influence of the ECC on the total energy of the TiNi single

ECC	ΔE
10^{-5}	3.69×10^{-3}
10^{-6}	7.80×10^{-5}
10^{-7}	2.53×10^{-6}
10^{-8}	0

ΔE : Difference from total energy calculated using the conditions of Ecc=10^{-8}

Table 6 Elastic interaction energy $E_{i\text{-}j}$ of twin

	Twinning plane	$E_{i\text{-}j}$(MJ/m^3)
A-c1	(1, 0, 0)	-623
A-c2	(0, $\bar{1}$, 1)	-485
B-i	(0, 0, $\bar{1}$)	-646
B-ii	(0.58, 0.81, 0)	-561
C-i	(1, 1, 0)	-622
C-ii	(0.30, 0.$\bar{3}$0, 0.91)	-579
D-i	(1, $\bar{1}$, 0)	-572
D-ii	(0.67, 0.67, 0.$\bar{3}\bar{3}$)	-52

Table 7 Interfacial energy of twin plane

	Twinning plane	γ (mJ/m^2)
A-c1	(1, 0, 0)	202
A-c2	(0, $\bar{1}$, 1)	356
B-i	(0, 0, $\bar{1}$)	136
B-ii	(0.58, 0.81, 0)	N/A
C-i	(1, 1, 0)	152
C-ii	(0.30, 0.$\overline{30}$, 0.91)	N/A
D-i	(1, $\bar{1}$, 0)	188
D-ii	(0.67, 0.67, 0.$\overline{33}$)	N/A

Table 8 Incompatibility in HPV pair

CV_i	CV_j	Group	No	Junction plane between HPVs			Major twin				Minor twin			
				$\mathbf{n}_{ij}$	θ (deg)	$\mathbf{\Gamma}$	$\mathbf{n}_{ij}$	θ (deg)	$\mathbf{\Gamma}$	Twin type	$\mathbf{n}_{ij}$	θ (deg)	$\mathbf{\Gamma}$	Twin type
	(1-2)	I	I-1	(0,1,0)	-11.33	[0.41,0,0.91]	(0,1,0)	-11.33	[0.41,0,0.91]	B-i	(0,1,0)	-11.33	[0.41,0,0.91]	B-i
			I-2	(-0.82,0.,0.57)	2.06	[0.75,0,-0.67]	(-0.59,0,0.81)	-8.78	[-0.99,0,0.17]	B-ii	(0.59,0,0.81)	17.67	[1.00,0,0.05]	B-ii
	(1'-2')	II	II-1	(0,0,1)	6.87	[0.24,0.97,0]	(0,0,1)	14.45	[0.61,0.80,0]	B-i	(0,0,1)	-18.80	[0.94,0.34,0]	B-i
			II-2	(-0.59,0.81,0)	-5.16	[0.87,-0.50,0]	(0.59,-0.81,0)	-5.16	[0.87,-0.50,0]	B-ii	(-0.59,0.81,0)	-5.16	[0.87,-0.50,0]	B-ii
	(2-1)	III	III-1	(1,0,0)	-2.85	[0,-0.88,0.47]	(1,0,0)	-2.85	[0,-0.88,0.47]	A-c1	(1,0,0)	-2.85	[0,-0.88,0.47]	A-c1
			III-2	(0,-0.89,-0.45)	-12.59	[0,-0.54,0.84]	(0,1,1)	-16.36	[0,-0.75,0.66]	A-c2	(0,1,-1)	-12.78	[0,0.63,0.78]	A-c2
	(2-1')	IV	IV-1	(0,1,1)	-12.48	[0.15,-0.70,0.70]	(0,1,1)	-16.46	[0.12,0.70,-0.70]	A-c2	Identity	11.38	[0.97,-0.16,0.16]	None
			IV-2	(1.00,0.05,-0.05)	-2.97	[0.40,-0.65,0.65]	(1,0,0)	-3.44	[0.60,0.56,-0.56]	A-c1				
(2'-1')	(2'-1)	V	V-1	(0,-1,1)	-2.84	[0.44,0.63,0.63]	Identity	2.24	[0.94,0.25,0.25]	None	(0,-1,1)	-16.88	[0.67,0.53,0.53]	A-c
			V-2	(0.98,0.14,0.14)	-1.97	[-0.90,0.31,0.31]					(1,0,0)	11.10	[-1.00,0.07,0.07]	A-c
	(3-4')	VI	VI-1	(1,1,0)	-10.56	[0.33,-0.33,0.89]	(1,1,0)	-10.56	[0.33,-0.33,0.89]	D-i	(1,1,0)	-10.56	[0.33,-0.33,0.89]	D-i
			VI-2	(-0.70,0.70,0.17)	-4.05	[0.64,-0.64,0.42]	(-0.67,0.67,0.33)	-2.74	[0.55,-0.55,0.62]	D-ii	(0.67,-0.67,0.33)	-7.96	[0.69,-0.69,0.22]	D-ii
	(4'-3)	VII	VII-1	(1,-1,0)	-2.20	[0.46,0.46,0.76]	(1,-1,0)	-2.20	[0.46,0.46,0.76]	C-i	(1,-1,0)	-2.20	[0.46,0.46,0.76]	C-i
			VII-2	(0.49,0.49,0.72)	-11.10	[0.35,0.35,-0.87]	(0.30,0.30,0.91)	-17.26	[0.58,0.58,-0.58]	C-ii	(0.30,0.30,-0.91)	-19.59	[0.64,0.64,0.44]	C-ii
	(5'-6)	VIII	VIII-1	(1,0,1)	-8.93	[0.16,0.97,-0.16]	(1,0,1)	-12.60	[0.38,0.85,-0.38]	D-i	(1,0,1)	11.88	[-0.69,0.24,0.69]	C-i
			VIII-2	(0.69,0.23,-0.69)	-4.01	[0.71,0.05,-0.71]	(-0.67,0.33,0.67)	-5.16	[0.58,0.57,-0.58]	D-ii	(0.30,0.91,-0.30)	-7.32	[-0.33,0.89,0.33]	C-ii
	(6'-5)	IX	IX-1	(1,0,-1)	0.23	[0.38,0.85,0.38]	(1,0,-1)	5.88	[0.63,0.46,0.63]	C-i	(1,0,-1)	-13.95	[0.64,0.44,0.64]	D-i
			IX-2	(0.42,0.80,0.42)	-13.57	[0.54,-0.65,0.54]	(0.30,0.91,0.30)	-15.18	[0.48,-0.74,0.48]	C-ii	(0.67,-0.33,0.67)	-10.70	[0.70,-0.17,0.70]	D-ii